Since January 2020 Elsevier has created a COVID-19 resource centre with free information in English and Mandarin on the novel coronavirus COVID-19. The COVID-19 resource centre is hosted on Elsevier Connect, the company's public news and information website.

Virology 383 (2009) 328–337

Contents lists available at ScienceDirect

Virology

journal homepage: www.elsevier.com/locate/yviro

Formation of stable homodimer via the C-terminal α-helical domain of coronavirus nonstructural protein 9 is critical for its function in viral replication

Bo Chen [a], Shouguo Fang [b], James P. Tam [a], Ding Xiang Liu [a,b,*]

[a] School of Biological Sciences, Nanyang Technological University, 60 Nanyang Drive, Singapore 637551, Singapore
[b] Institute of Molecular and Cell Biology, 61 Biopolis Drive, Proteos, Singapore 138673, Singapore

ARTICLE INFO

Article history:
Received 14 August 2008
Returned to author for revision
5 September 2008
Accepted 23 October 2008
Available online 20 November 2008

Keywords:
Coronavirus
Non-structural protein 9
Dimerization
RNA-binding
Viral replication

ABSTRACT

Coronaviruses devote more than three quarters of their coding capacity to encode two large polyproteins (1a and 1ab polyproteins), which are proteolytically processed into 15–16 mature, nonstructural replicase proteins (nsp1 to 16). These cleavage products are believed to play essential roles in replication of the giant RNA genome of ~30 kb and transcription of a nested set of 5 to 9 subgenomic RNA species by a unique discontinuous transcription mechanism. In this report, one of these replicase proteins, nsp9 of the coronavirus infectious bronchitis virus (IBV) is systematically studied using both biochemical and reverse genetic approaches. The results showed that substitution mutation of a conserved Gly (G98) residue in the C-terminal α-helix domain with an Asp greatly destabilized the IBV nsp9 homodimer and abolished its RNA-binding activity. Introduction of the same mutation into an infectious IBV clone system showed that the mutation totally abolishes the transcription of subgenomic RNA and no infectious virus could be recovered. Mutation of a semi-conserved Ile (I95) residue in the same region showed moderately destabilizing effect on the IBV nsp9 homodimer but minimal effect on its RNA-binding activity. Introduction of the mutation into the IBV infectious clone system showed recovery of a mutant virus with severe growth defects, supporting that dimerization is critical for the function of this replicase protein. Meanwhile, mutations of some positively charged residues in the β-barrel regions of the IBV nsp9 protein significantly reduced its RNA-binding activity, but with no obvious effect on dimerization of the protein. Introduction of these mutations into the viral genome showed only mild to moderate effects on the growth and infectivity of the rescued mutant viruses.

Introduction

Coronavirus is a family of RNA viruses with the largest RNA genome known so far. In cells infected with coronavirus, a nested set of genomic and subgenomic RNA species is produced and used for translation of viral structural and nonstructural proteins. Among these proteins, the 1a and 1ab polyproteins are post-translationally processed to smaller, mature proteins (Ziebuhr et al., 2000; Ziebuhr, 2005). It is generally believed that replication of the large RNA genome and transcription of a nested set of 5 to 8 subgenomic RNA species are carried out by these replicase proteins. However, the exact functions of individual replicase proteins are largely unknown. In recent years, determination of the crystal structures of some of these proteins, including the proteinase domain of nsp3, nsp5, nsp7 and 8, nsp9, nsp10 and nsp15, led to the revelation of many important functions for these proteins (Saikatendu et al., 2005; Ratia et al., 2006; Peti et al., 2005; Zhai et al., 2005; Anand et al., 2002, 2003; Yang et al., 2003; Egloff et al., 2004; Sutton et al., 2004; Su et al., 2006; Joseph et al., 2006; Ricagno et al., 2006), but most of these functions are not rigorously tested in a biologically relevant system. In this study, residues critical for dimerization and the RNA-binding activity of nsp9 protein from coronavirus infectious bronchitis virus (IBV) were systematically studied by mutagenesis, based on the structural studies of SARS-CoV nsp9 protein.

IBV is a group 3 coronavirus. Its genome contains a 27.6 kb single-stranded, positive-sense RNA. In the virus-infected cells, six mRNA species, including the genome-length mRNA 1 and five subgenomic mRNAs (mRNA 2–6), are produced, and each mRNA species possesses a 64 nucleotides leader sequence derived from the 5′-end of the genome (Boursnell et al., 1987). Subgenomic mRNAs 2, 3, 4, and 6 encode the four structural proteins, i.e., spike glycoprotein (S), envelope protein (E), membrane protein (M) and nucleocapsid protein (N). The 5′-two-third region of mRNA 1 encodes the 1a and 1ab polyproteins, which are proteolytically cleaved by two virus-encoded proteinases, the papain-like and 3C-like proteinases, into at least 15 nonstructural proteins (nsp2–nsp16) (Lim and Liu, 1998a, 1998b; Lim et al., 2000; Liu et al., 1995, 1997, 1998; Ng and Liu, 1998, 2000, 2002; Xu et al., 2001).

A cluster of small proteins, i.e., nsp7, nsp8, nsp9 and nsp10, is located at the C-terminal region of the la polyprotein. The functional roles of these proteins in coronavirus RNA replication and transcription

* Corresponding author. Fax: +65 67791117.
E-mail address: dxliu@imcb.a-star.edu.sg (D.X. Liu).

0042-6822/$ – see front matter © 2008 Elsevier Inc. All rights reserved.
doi:10.1016/j.virol.2008.10.032

are emerging via biochemical and structural analysis. For example, the SARS-CoV nsp8 protein was recently shown to have a non-canonical RNA-dependent RNA polymerase (RdRp) activity (Imbert et al., 2006). Most of the replicase products could be assembled into a membrane-associated viral replication/transcription complex (Sims et al., 2000; Gosert et al., 2002; Prentice et al., 2004; Shi et al., 1999; Bost et al., 2000; Masters 2006; Brockway et al., 2003).

Determination of the crystal structure of SARS-CoV nsp9 protein shows that it forms a homodimer (Egloff et al., 2004; Sutton et al., 2004). Searching for structural homology between SARS-CoV nsp9 and other RNA binding proteins suggests that the SARS-CoV nsp9 protein is a nucleic acid-binding protein and has nonspecific RNA-binding activity (Egloff et al., 2004). Biophysical evidence has also shown an interaction between SARS-CoV nsp9 and nsp8 proteins (Sutton et al., 2004). Based on sequence comparison, a number of evolutionarily conserved amino acid residues in different domains of the IBV nsp9 protein were systematically mutated to assess their roles in viral replication and infectivity by introducing into an infectious cDNA clone system derived from the genomic RNA of IBV. Subsequently, dimerization and the RNA-binding activity of the purified wild type and mutant IBV nsp9 protein were studied by immunoprecipitation, gel filtration, chemical cross linking and Northwestern blotting. These studies led to the identification of amino acid residues essential for dimerization and the RNA-binding activity of IBV nsp9 protein. This study thus presents biochemical and genetic evidence that directly links dimerization and the RNA binding activity of the coronavirus nsp9 protein to virus replication and infectivity in cultured cells. This information would be of help in design of preventive and treatment approaches against coronavirus infection.

Results

Introduction of single amino acid substitutions into the IBV genome and analysis of their effect on the replication and infectivity of IBV

Multiple alignment of the nsp9 sequences from IBV (accession No. NP-040829) and SARS-CoV (accession No. AY291315) shows that the two proteins share 70% similarity at the amino acid level (Fig. 1a).

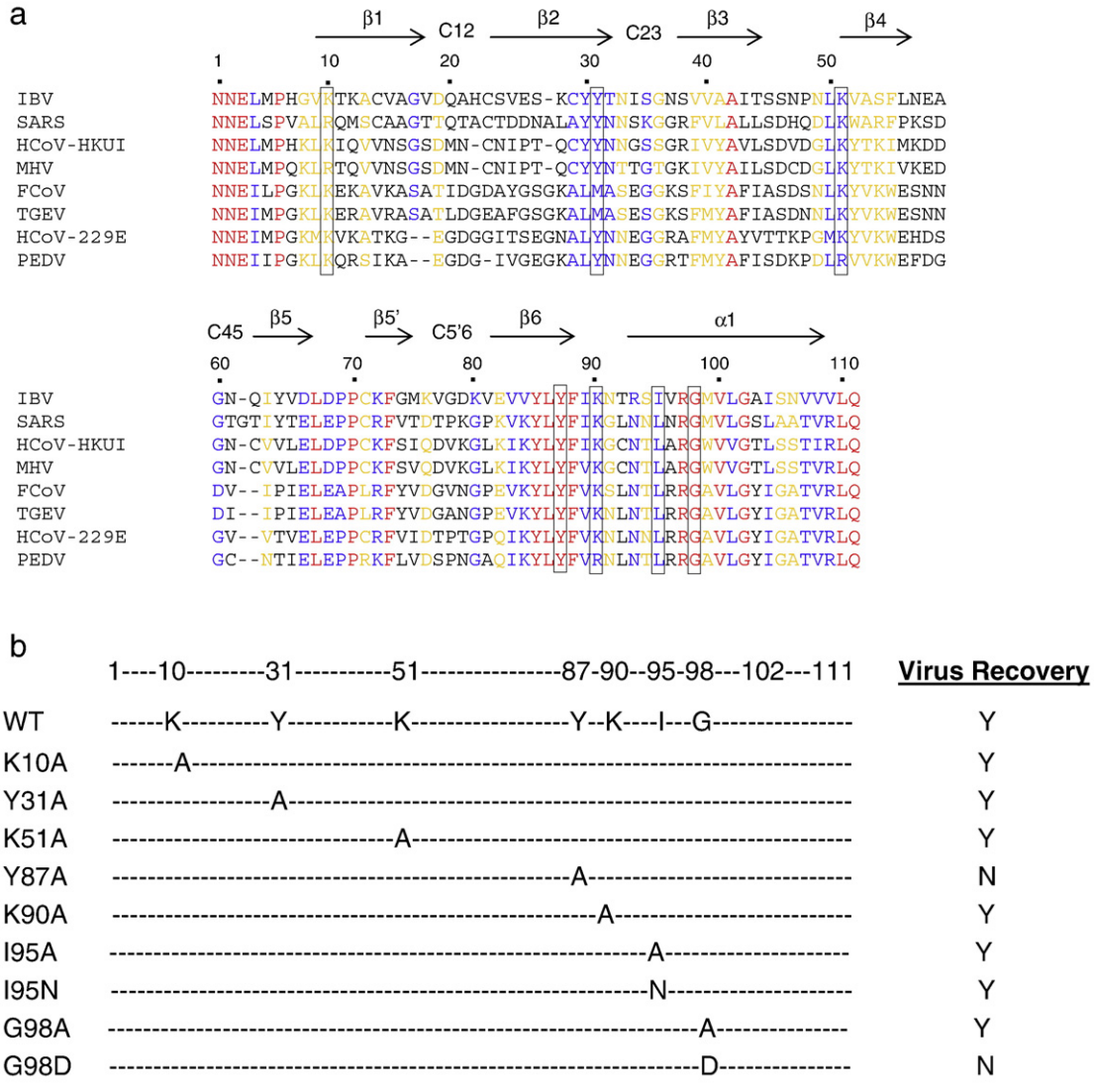

Fig. 1. Mutational analysis of the IBV nsp9 protein. (a) Structure-based alignment of coronavirus nsp9 protein. Secondary structure elements are labeled above the sequence for IBV, based on the structure of SARS-CoV nsp9 protein. Sequences of IBV (infectious bronchitis virus, strain Beaudette, NP_040838); H-CoV (Human Coronavirus, strain HKU1, YP_173242); MHV (Murine Hepatitis Virus, strain 1, AAA46439); TGEV (Porcine Transmissible Gastroenteritis Virus, strain RM4, AAG30228); and SARS (SARS-Coronavirus, 1SSK_A) were obtained from GenBank. The identical amino acid residues in all eight coronavirus species are marked in red, the residues for which conservation is above 70% are marked in blue and above 60% are marked in yellow. The amino acid residues chosen for mutational analysis in this study are boxed. (b) Diagram showing the mutations introduced into the IBV nsp9 protein. Also shown is the summary of virus recovery from wild type and mutant transcripts.

Systematic mutagenesis of the IBV nsp9 protein was carried out to identify amino acid residues critical for the dimerization and the RNA-binding activity of the protein. The effect of these mutations on the infectivity and replication of IBV was studied by using an infectious IBV cloning system.

Nine point mutations, K10A, Y31A, K51A, Y87A, K90A, I95A, I95N, G98A and G98D (Fig. 1a), were made and introduced separately into the infectious IBV clone. The in vitro transcribed full-length RNA derived from wild type and the mutant constructs were generated by in vitro transcription using the T7 RNA polymerase in the presence of a cap analog. Electroporation of wild type RNA transcripts together with an RNA fragment covering the N protein region into Vero cells showed the formation of massive cytopathic effect (CPE) at 2 days post-electroporation (Fig. 1b and data not shown). Similarly, typical CPEs were observed in cells transfected with mutant transcripts derived from K10A, Y31A, K51A, K90A, I95A, and G98A constructs at 2 days post-electroporation and recombinant viruses were recovered (Fig. 1b). In cells electroporated with the I95N transcripts, a typical CPE was observed at 3 days post-electroporation (Fig. 1b). Re-infection of fresh Vero cells with medium collected from total cell lysates prepared by freezing and thawing cells transfected with these mutant transcripts showed the formation of typical CPE, indicating that the mutant viruses rescued from the initially transfected cells maintain infectivity in subsequent passages.

In contrast, no CPE formation was observed in cells transfected with transcripts derived from Y87A and G98D mutant constructs up to 5 days post-electroporation in four repeated experiments (Fig. 1b). Subsequent infection of fresh cells with cell lysate preparations by freezing and thawing the initially transfected cells showed no sign of IBV infection, as judged by CPE formation and Western blot analysis (data not shown), suggesting that no infectious virus could be rescued from these mutant transcripts. These results indicate that Y87A and G98D mutations may abolish the infectivity of the in vitro synthesized full-length IBV transcripts.

As the C-terminal domain may play an essential role in dimerization of nsp9 protein and dimerization was thought to be critical for its RNA binding activity, the effects of mutations in the C-terminal region were firstly characterized in the following studies.

Characterization of the phenotypic and growth properties of the rescued I95A, I95N and G98A mutant viruses, and analysis of negative-strand RNA replication and subgenomic RNA transcription in cells transfected with G98D mutant transcripts

The growth properties of I95A, I95N and G98A mutant viruses on Vero cells were tested by analysis of plaque sizes and growth curves of the passage 3 mutant viruses. As shown in Fig. 2a, very similarly sized plaques were observed in cells infected with wild type (rIBV) and the mutant viruses. Analysis of the growth curves of wild type and mutant viruses demonstrated that the I95A and G98A mutant viruses exhibited similar growth kinetics as wild type virus, reaching the peak at 16 h post-infection (Fig. 2a). At this time point, the titers of the two mutant viruses were approximately 2–3 fold lower than that of wild type virus (Fig. 2a). The I95N mutant virus grew more slowly than wild type virus, reaching the peak at 24 h post-infection (Fig. 2a). The titer of this mutant virus was approximately 100 fold lower than that of wild type virus (Fig. 2a).

As no infectious virus was recovered from cells transfected with G98D mutant transcripts, total RNA was extracted from cells electroporated with wild type and mutant full-length transcripts, and RT-PCR amplification of negative strand RNA was performed to check if RNA replication occurred in these transfected cells. The primer pair was chosen so that the IBV sequence from nucleotides 14,931 to 15,600 would be amplified by the RT-PCR reaction. If replication of viral RNA occurred, a 670 bp PCR fragment would be expected. As shown in Fig. 2b, RT-PCR fragments amplified from both positive (lanes 2 and 5) and negative (lanes 3 and 6) strand RNA templates were obtained from cells transfected with wild type and the mutant transcripts. The amount of negative strand RNA was approximately one third of the positive strand RNA (Fig. 2b). RT-PCR amplification of subgenomic mRNAs was then carried out to check whether a low level of subgenomic mRNA transcription occurred in cells transfected with the mutant transcripts. The forward primer used in this reaction corresponds to the leader sequence from nucleotides 26–46 in the genomic RNA and the downstream primers covers IBV sequences from nucleotides 24,784 to 24,803. If transcription of subgenomic mRNAs did occur, a 415 bp PCR product corresponding to the 5′-terminal region of the subgenomic

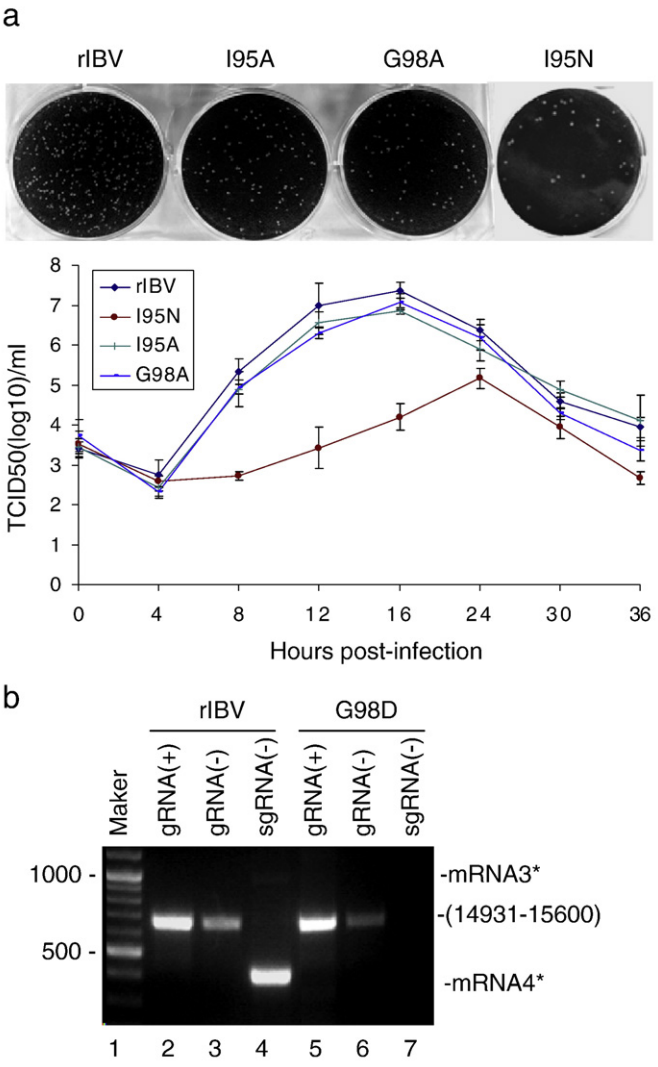

Fig. 2. Analysis of the growth properties of wild type, and I95A, I95N and G98A mutant viruses. (a) Plague sizes (upper panels) and growth curves (lower panel) of wild type and I95A, I95N and G98A mutant viruses. Monolayers of Vero cells on a 6-well plate were infected with 100 μl of 1000-fold diluted virus stock and cultured in the presence of 0.5% carboxymethy cellulose at 37 °C for 3 days. The cells were fixed and stained with 0.1% toluidine. Vero cells were infected with wild type and mutant viruses, and harvested at 0, 4, 8, 12, 16, 24, 30 and 36 h post-inoculation, respectively. Viral stocks were prepared by freezing/thawing of the cells three times and TCID50 of each viral stock was determined by infecting five wells of Vero cells on 96-well plates in triplicate with 10-fold serial dilution of each viral stock. (b) Analysis of RNA replication in cells electroporated with wild type and G98D mutant transcripts. Total RNA was prepared from Vero cells electroporated with in vitro synthesized full-length transcripts three days post-electroporation. Regions corresponding to nucleotides 14,931–15,600 of the positive (+) and negative (−) sense IBV genomic RNA were amplified by RT-PCR and analyzed on 1.2% agarose gel (lanes 2–3 and 5–6). The negative sense, subgenomic mRNA 4 was also amplified and analyzed (lanes 4 and 7). Lane 1 shows DNA markers. Numbers on the left indicate nucleotides in bases.

mRNA4 and a 1010 bp fragment corresponding to the 5′-terminal region of the subgenomic mRNA3 would be expected. As shown in Fig. 2b, a dominant 415 bp band and a weak 1010 bp band were observed in cells electroporated with wild type full-length transcripts at two days post-electroporation (lane 4). However, the same PCR products were not detected in cells electroporated with the mutant transcripts at 72 h post-electroporation (Fig. 2b, lane 7).

Destabilization of the IBV nsp9 homodimer by introducing point mutations into the C-terminal region correlating with the defect of I95N and G98D mutant constructs in viral RNA replication and infectivity

Biochemical analysis of the effect of I95A, I95N, G98A and G98D mutations on the dimerization and RNA-binding activity of the IBV nsp9 was then carried out to understand the detailed mechanisms of these point mutations on the replication and infectivity of IBV. For this purpose, wild type and mutant fragments with a 6-His tag at their N-terminus were cloned into a bacterial expression vector, expressed in *E. coli* and purified to near homogeneity. After removing the 6-His tag, the purified proteins were treated with 0–2% of glutaraldehyde, a short self-polymerizing reagent that reacts with lysine, tyrosine, histidine and tryptophan residues, and analyzed by SDS-PAGE. Gradually increased detection of the homodimer was observed following cross-linking of wild type and mutant proteins with increasing concentrations of the cross-linking agent (Fig. 3a). Interestingly, it was noted that G98D mutant protein showed much less, if any, dimer formation without cross-linking with glutaraldehyde (Fig. 3a). The I95N mutant protein also showed significantly reduced dimer formation under the same conditions (Fig. 3a). These results suggest that the I95N and G98D mutations may destabilize the IBV nsp9 homodimer.

This possibility was further studied in the following two ways. First, the purified wild type and mutant proteins were analyzed by gel filtration after removing the 6-His tag. The results showed the detection of two peaks for wild type and the I95N mutant (Fig. 3b). Analysis of the two peaks by mass spectrometry confirmed that they indeed represent the nsp9 monomers and dimers, respectively. However, only one peak was observed for the G98D mutant protein (Fig. 3b). Once again, analysis by mass spectrometry confirmed that it represents the nsp9 monomers containing the right point mutation. Second, wild type, I95N and G98D mutant nsp9 were cloned into a mammalian expression vector with either a Flag or a Myc tag at the N-terminus. The Flag-tagged wild type nsp9 were co-expressed with the Myc-tagged wild type nsp9, I95N and G98D mutants, respectively. The association of wild type nsp9 protein with either wild type or mutant nsp9 proteins was analyzed by coimmunoprecipitation experiment with anti-Flag antibody. The immunoprecipitated proteins were separated on SDS-PAGE and analyzed by Western blotting with either anti-Flag or anti-Myc antibody. As shown in Fig. 3c, Western blot analysis of total cell lysates showed the detection of similar amounts of wild type and mutant nsp9 proteins either expressed on their own or co-expressed with the Flag-tagged wild type nsp9 (Fig. 3c, top panel). Analysis of the precipitates with anti-Flag antibody showed the presence of approximately equal amounts of the Flag-tagged wild type nsp9 either expressed on its own or co-expressed with the Myc-tagged wild type and mutant nsp9 (Fig. 3c, middle panel). Analysis of the same precipitates with anti-Myc antibody showed that efficient

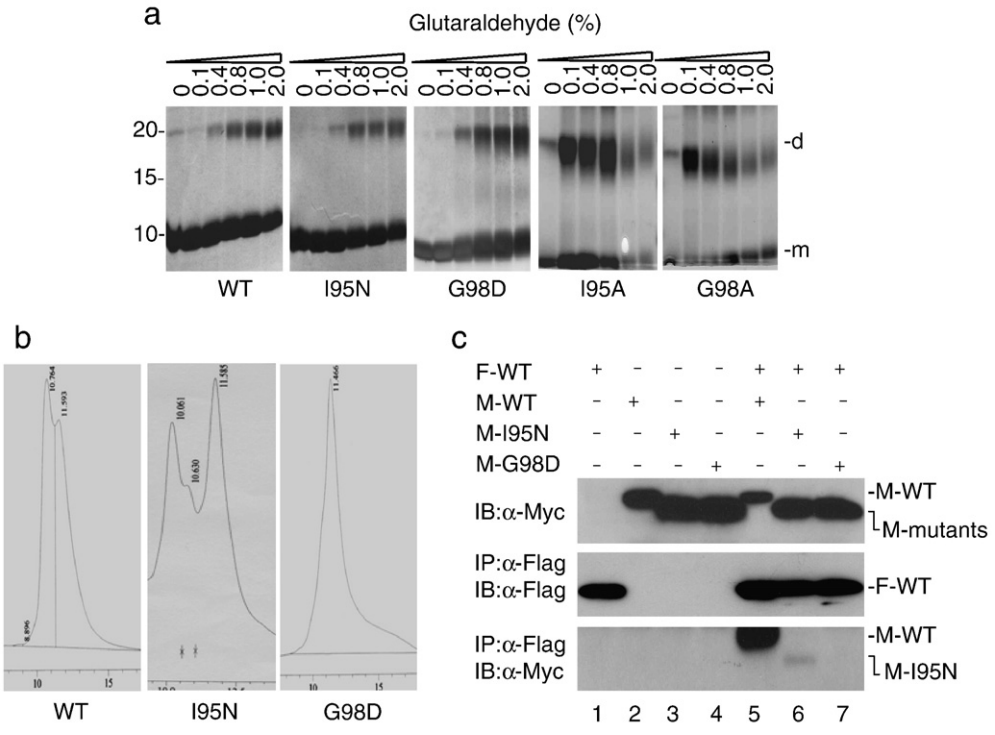

Fig. 3. Biochemical characterization of the dimerization of wild type, I95A, I95N, G98A and G98D mutant IBV nsp9 protein. (a) Analysis of dimerization of wild type and I95A, I95N, G98A and G98D mutant IBV nsp9 protein after chemical cross-linking. The purified wild type and mutant nsp9 proteins were treated with 0–2% of glutaraldehyde, and analyzed by SDS-15% polyacrylamide gel. The monomeric (m) and dimeric (d) forms of the protein are indicated. Numbers on the left indicate molecular masses in kiloDalton. (b) Analysis of wild type and I95N and G98D mutant nsp9 proteins by gel-filtration. The purified wild type and mutant nsp9 proteins were analyzed by gel filtration assay using BioSuiteTM 250 HR SEC column (7.8×300 mm, Waters) on Shimadszu chromatograph (LC-10ATvp) equipped with a photodiode array detector (SPD-M20A). The column was equilibrated at a flow rate of 1 ml/min with PBS buffer at room temperature. The protein samples (300 μl) were injected at a given concentration and detected. The first peak was formed by the nsp9 dimer (~24 kDa), and the second peak indicated the monomer (~12 kDa). (c) Analysis of the dimerization of wild type and I95N and G98D mutant proteins by co-immunoprecipitation. HeLa cells overexpressing the Flag-tagged wild type, Myc-tagged wild type and mutant nsp9 protein either on their own (lanes 1–4) or in different combination (lanes 5–7) were lysed, separated on SDS-15% polyacrylamide gel and analyzed by Western blotting with anti-Myc antibody (top panels). The same lysates were immunoprecipitated with anti-Flag antibody, separated on SDS-15% polyacrylamide gel and analyzed by Western blotting with either anti-Flag (middle panel) or anti-Myc (bottom panel) antibodies.

detection of the Myc-tagged wild type nsp9 was made only when it was co-expressed with the Flag-tagged nsp9 protein (Fig. 3c, bottom panel, lane 5). Interestingly, much reduced detection of the Myc-tagged I95N was observed when it was co-expressed with the Flag-tagged wild type nsp9 (Fig. 3c, bottom panel, lane 6), demonstrating that this point mutation destabilizes the nsp9 homodimer. When the Myc-tagged G98D construct was co-expressed with the Flag-tagged wild type nsp9, the mutant protein was not detected in the co-immunoprecipitation experiment (Fig. 3c, bottom panel, lane 7). Taken together, these results confirm that the G98D mutation totally abolishes the nsp9 homodimer formation.

Analysis of the effect of point mutations in the C-terminal region on the RNA-binding activity of IBV nsp9 protein

The effect of these mutations on the single strand RNA-binding activity of IBV nsp9 was then investigated by Northwestern blotting. Approximately equal amounts of the purified wild type and G98D mutant proteins were separated on SDS-PAGE either before or after removal of the 6-His tag (Fig. 4a, top panel). Once again, formation of reasonable amounts of dimer was detected in the purified wild type protein (Fig. 4a, top panel, lane 3). After transfer to a Hybond C extra membrane, the RNA-binding activities of wild type and G98D mutant proteins were analyzed by Northwestern blot with two probes corresponding, respectively, to the positive- and negative-sense 3′-UTR of IBV. The results showed that both wild type and G98D mutant proteins with the 6-His tag could efficiently bind to either probe (Fig. 4a, middle and bottom panels, lanes 1 and 2). It was noted that efficient detection of the dimeric form of the two proteins was achieved when either probe was used (Fig. 4a, middle and bottom panels, lanes 1 and 2), suggesting preferential binding of the probes to the homodimer of the protein. After removal of the 6-His tag, both the monomeric and dimeric forms of the purified wild type protein could still efficiently bind to either probe (Fig. 4a, middle and bottom panels, lane 3). However, very weak, if any, binding of the G98D mutant protein to either probe was observed after removal of the 6-His tag (Fig. 4a, middle and bottom panels, lane 4), suggesting that this point mutation abolishes the RNA-binding activity of IBV nsp9 protein. The other three mutant proteins showed similar RNA-binding activity as wild type protein, except that G98A mutant showed greatly reduced binding activity to the negative RNA probe (Fig. 4a, lane 7). The binding efficiency of wild type and the four mutant proteins was then quantified by densitometry measurement of bands from three independent experiments. The relative RNA-binding efficiencies of the mutant proteins to wild type protein are shown in Fig. 4b. The results demonstrated that the G98D mutant protein maintained 0 and 4% binding efficiencies, and the G98A mutant showed 75 and 10% binding efficiencies to the positive and negative probes, respectively (Fig. 4b). The I95A and I95N mutant proteins showed 80 to 100% binding efficiencies to both probes (Fig. 4b).

Biochemical and functional characterization of the effects of K10A, Y31A, K51A, Y87A and K90A mutations on dimerization and RNA-binding activity of IBV nsp9 protein

Biochemical characterization of the effects of other five mutations (K10A, Y31A, K51A, Y87A and K90A) on the dimerization and RNA-binding activity of IBV nsp9 protein was then carried out. The K10A, Y31A, K51A and K90A mutant proteins were successfully expressed in bacteria and purified to near homogeneity. Efforts were made to express the Y87A mutant protein in the same system. However, very low, if any, expression of the mutant protein was consistently observed for some unknown reasons (data not shown). This mutant construct was not included in the subsequent studies. After removing the 6-His tag, the purified proteins were treated with 0–2% of glutaraldehyde and analyzed by SDS-PAGE, showing gradually

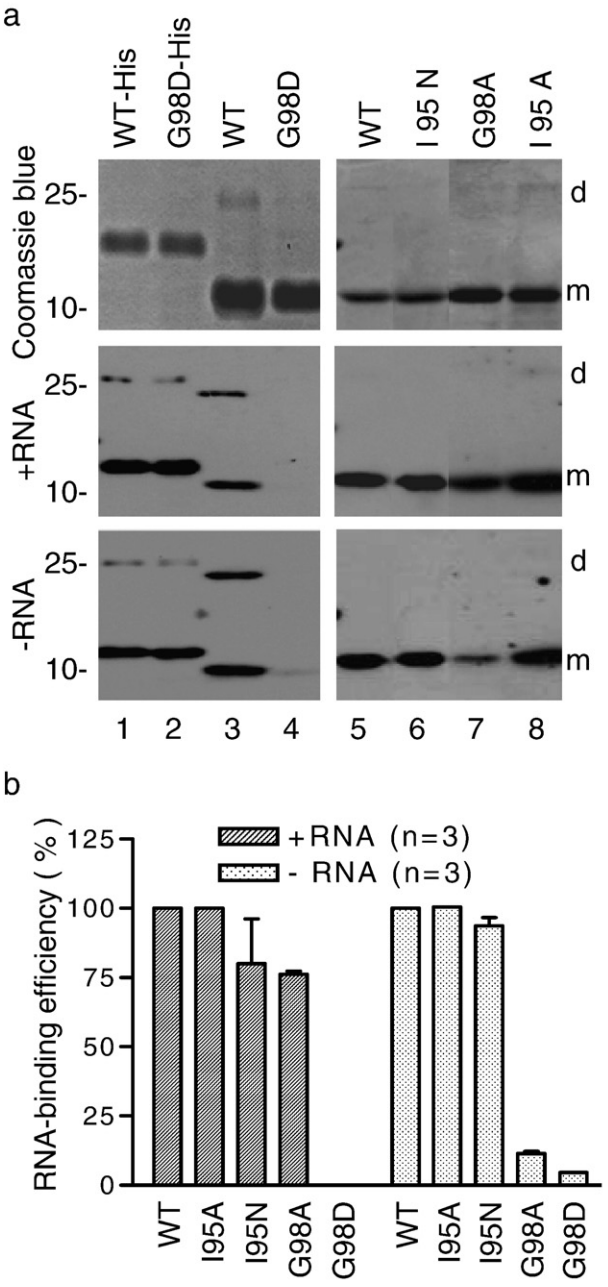

Fig. 4. Analysis of the RNA-binding activity of wild type and I95A, I95N, G98A and G98D mutant IBV nsp9 proteins. (a) Northwestern analysis of the RNA binding activity of wild type and I95A, I95N, G98A and G98D mutant nsp9 proteins. The purified wild type and mutant nsp9 proteins with or without the 6xHis tag were separated on two SDS-15% polyacrylamide gels. One gel was directly detected by staining with Commassie blue (top panel), and the second was transferred to Hybond C extra membrane. The RNA-binding activity was probed with either positive (middle panel) or negative (bottom panel) sense, digoxin-labeled RNA corresponding to 26,539–27,608 nucleotides of the IBV genome. The bands corresponding to the dimeric form with the His tag (d-His), the dimeric form without the His tag (d), the monomeric form with His tag (m-His) and the monomeric form without the His tag (m) are indicated. Numbers on the left indicate molecular masses in kiloDalton. (b) The relative binding activities of wild type and I95A, I95N, G98A and G98D mutant nsp9 proteins to either positive or negative sense probes were quantified by densitometry measurement of individual bands in three independent Northwestern blot experiments, as shown above. The binding activity of wild type nsp9 protein to both probes was treated as 100%.

increased detection of the homodimer following cross-linking of wild type and mutant proteins with increasing concentrations of the cross-linking agent (Fig. 5a). Analysis of the purified proteins by gel filtration showed the presence of two peaks for wild type and the mutant proteins (Fig. 5a).

The RNA-binding activity of wild type and the mutant proteins was then analyzed by Northwestern blot in three independent experiments. As a representative gel shown in Fig. 5b, the K10A and K90A mutations greatly reduced the RNA-binding activity to either probe (lanes 2 and 5). The K51A mutant protein showed moderately reduced binding activity (Fig. 5b, lane 4), and the Y31A mutant protein showed marginally reduced binding activity (Fig. 5b, lanes 3 and 6). Quantification by densitometry measurement of bands from three independent experiments showed that the K10A and K90A mutants maintained approximately 10% binding efficiency to either probe, the

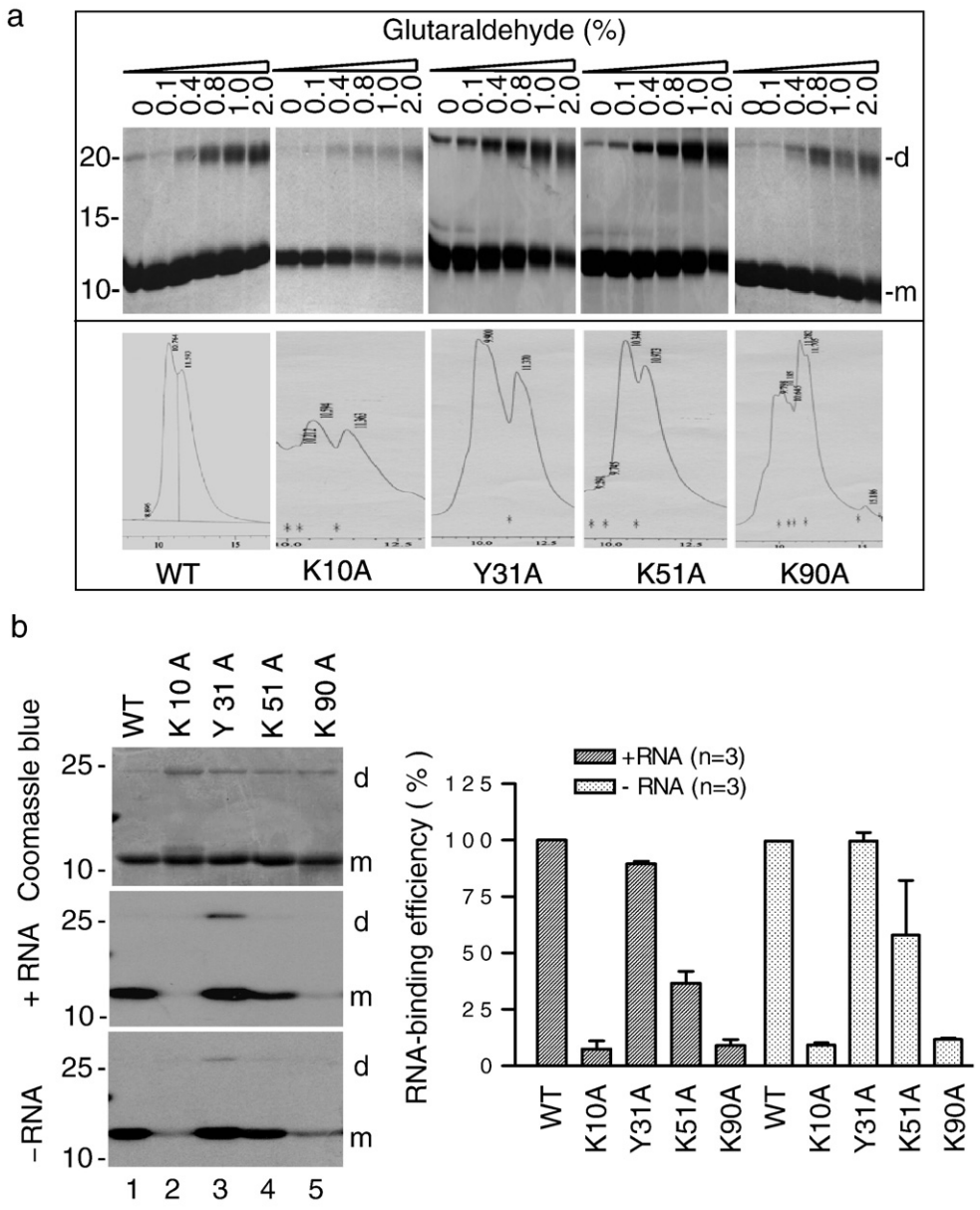

Fig. 5. Biochemical and functional analysis of the effects of K10A, Y31A, K51A and K90A mutations on dimerization and RNA-binding activity of IBV nsp9 protein as well as the growth properties of the recovered mutant viruses. (a) Analysis of dimerization of wild type mutant IBV nsp9 protein after chemical cross-linking (upper panels) and by gel-filtration (lower panels). The purified wild type and mutant nsp9 proteins were treated with 0–2% of glutaraldehyde, and analyzed by SDS-15% polyacrylamide gel. The monomeric (m) and dimeric (d) forms of the protein are indicated. Numbers on the left indicate molecular masses in kiloDalton. The purified wild type and mutant nsp9 proteins were also analyzed by gel filtration assay using BioSuiteTM 250 HR SEC column (7.8×300 mm, Waters) on Shimadszu chromatograph (LC-10ATvp) equipped with a photodiode array detector (SPD-M20A). The column was equilibrated at a flow rate of 1 ml/min with PBS buffer at room temperature. The protein samples (300 μl) were injected at a given concentration and detected. The first peak was formed by the nsp9s dimer (~24 kDa), and the second peak the monomer (~12 kDa). (b) Analysis of the RNA-binding activity of wild type and mutant IBV nsp9 protein. Northwestern analysis of the RNA binding activity of wild type and K10A, Y31A, K51A and K90A mutant nsp9 proteins. The purified wild type and mutant nsp9 proteins without the 6xHis tag were separated on two SDS-15% polyacrylamide gels. One gel was directly detected by staining with Commassie blue (left column, top panel), and the second was transferred to Hybond C extra membrane. The RNA-binding activity was probed with either positive (left column, middle panel) or negative (left column, bottom panel) sense, digoxin-labeled RNA corresponding to 26,539–27,608 nucleotides of the IBV genome. The bands corresponding to the dimeric form without the His tag (d) and the monomeric form without the His tag (m) are indicated. Numbers on the left indicate molecular masses in kiloDalton. The relative binding activities of wild type and mutant nsp9 protein to either positive or negative sense probes were quantified by densitometry measurement of individual bands in three independent Northwestern blot experiments, as shown above (right column). The binding activity of wild type nsp9 protein to both probes was treated as 100%. (c) Plaque sizes (top panels) and growth curves (lower panel) of wild type and K10A, Y31A, K51A and K90A mutant viruses. Monolayers of Vero cells on a 6-well plate were infected with 100 μl of 1000-fold diluted virus stock and cultured in the presence of 0.5% carboxymethy cellulose at 37 °C for 3 days. The cells were fixed and stained with 0.1% toluidine. Vero cells were infected with wild type and K10A, Y31A, K51A and K90A mutant viruses, and harvested at 0, 4, 8, 12, 16, 24, 30 and 36 h post-inoculation, respectively. Viral stocks were prepared by freezing/thawing of the cells three times and TCID50 of each viral stock was determined by infecting five wells of Vero cells on 96-well plates in triplicate with 10-fold serial dilution of each viral stock.

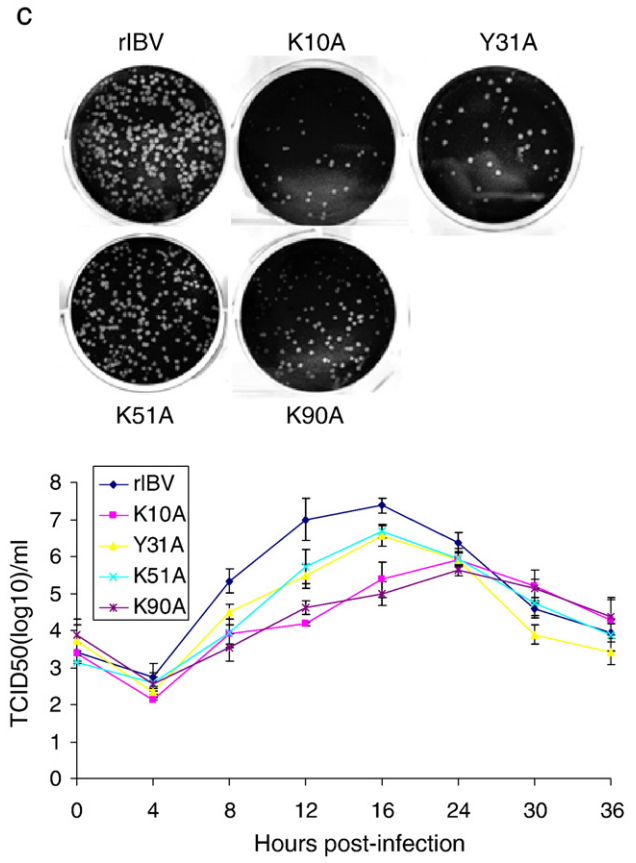

Fig. 5 (*continued*).

K51A mutant protein approximately 35 and 55% binding efficiencies to the positive and negative probes, respectively, and the Y31A and I95N mutant proteins 80 to 100% binding efficiencies to both probes (Fig. 5c).

The growth properties of the recovered K10A, Y31A, K51A and K90A mutant viruses on Vero cells were tested by analysis of plaque sizes and growth curves of the passage 3 mutant viruses. As shown in Fig. 6c, very similarly sized plaques were observed in cells infected with wild type (rIBV) and Y31A and K51A mutant viruses. In cells infected with K10A and K90A and mutant viruses, plaques with slightly smaller size were observed (Fig. 5c). Analysis of the growth curves of wild type and mutant viruses demonstrated that the Y31A and K51A exhibited similar growth kinetics as wild type virus, reaching the peak at 16 h post-infection (Fig. 5c). At this time point, the titers of the two mutant viruses were approximately 5 fold lower than that of wild type virus (Fig. 5c). The other two mutant viruses, K10A and K90A, grew slightly more slowly than wild type virus, reaching the peak at 24 h post-infection (Fig. 5c). The titers of these mutant viruses were approximately 20 fold lower than that of wild type virus (Fig. 5c).

Discussion

Coronavirus encodes two large polyproteins (1a and 1ab polyproteins) by the genome-length mRNA, mRNA1. It is generally believed that the functionally active form of the coronavirus replicase proteins would consist of 15–16 smaller, mature proteins (nsp1–nsp16) derived by proteolytic cleavage of these two polyproteins. In this study, systematic mutagenesis of one of these proteins, nsp9, was carried out to study the functional roles of this protein in coronavirus RNA replication and infectivity. Our results are consistent with structural data that indicate that nsp9 forms homodimers, and we have identified residues that are essential for nsp9 function during virus replication. Substitution of a negatively charged amino acid (Asp) for a conserved G98 residue in the C-terminal α-helix greatly destabilized the IBV nsp9 homodimer and abolished the RNA-binding activity of the protein. Consequently, introduction of the same mutation into the infectious IBV clone system showed that the mutation abolished the transcription of subgenomic RNA and no infectious virus could be rescued. Interestingly, mutation of a semi-conserved Ile (I95) residue in the same region showed minimal effect on the RNA-binding activity of the protein and moderately destabilizing effect on the homodimer. Introduction of this mutation into the IBV infectious clone system showed the recovery of a mutant virus with severe growth defects, supporting that dimerization is critical for the function of this replicase protein.

In previous structural studies, the crystal structure of SARS-CoV nsp9 crystal contains a dimer in the asymmetric unit (Fig. 6). In each monomer, seven-β strands and one α-helix form a cone-shaped β-barrel flanked by the C-terminal α-helix (Fig. 6). The C-terminal α-helix has a high content of hydrophobic residues, yielding two hydrophobic sides.

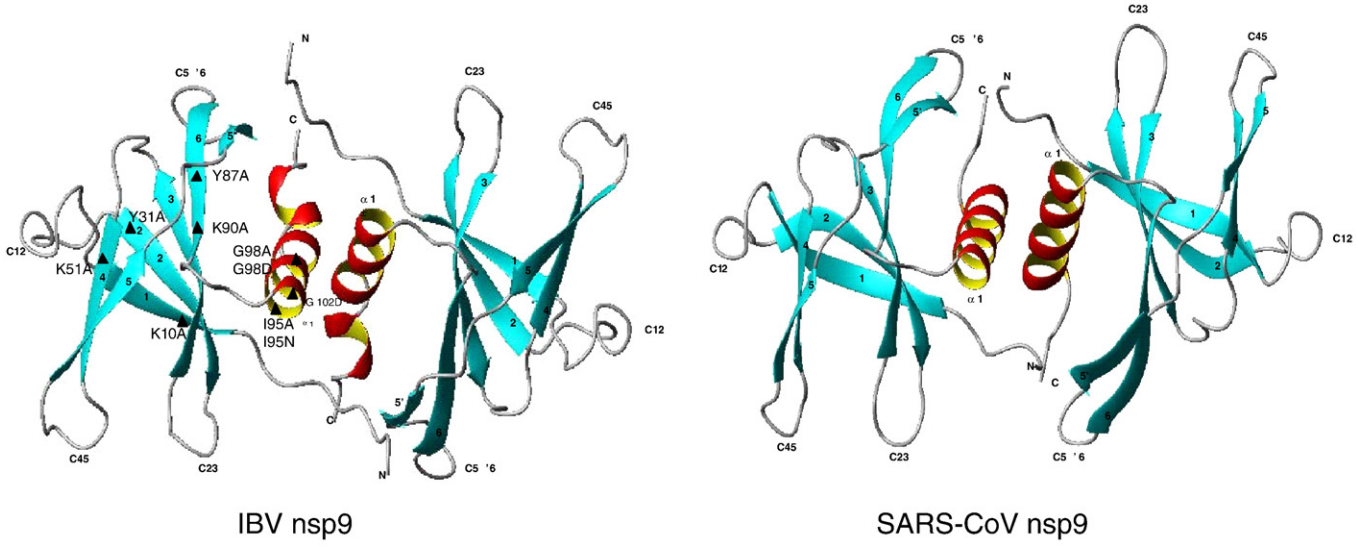

Fig. 6. Structural model of IBV nsp9 protein. The ribbon representation of IBV and SARS-CoV nsp9 protein is shown. The IBV nsp9 structure was presented based on structural modeling.

One side faces the β-barrel and the other interacts with the C-terminal α-helix of the second crystallographic monomer to form the homodimer (Fig. 6). This homodimer is therefore assembled by hydrophobic interactions (Egloff et al., 2004; Sutton et al., 2004). Analysis of the purified SARS-CoV nsp9 protein by surface plasmon resonance demonstrated that it is a single strand RNA-binding protein (Egloff et al., 2004). This single strand RNA-binding activity was further confirmed by fluorescence experiments (Egloff et al., 2004). By structural modeling, the IBV nsp9 protein was found to adopt a very similar folding as the SARS-CoV nsp9 protein (Fig. 6). Based on these structural studies, the topology of nsp9 protein was shown to most closely resemble the domains of the 3C-like proteinase ($3CL^{pro}$) which belongs to the serine proteinase superfamily (Berman et al., 2000). Structure alignments revealed that it best matches to the domain II of the coronavirus $3CL^{pro}$ and subdomian I of the picornaviral $3C^{pro}$, suggesting that the two groups of proteins may share certain evolutionary relationship and may play some regulatory functions (Sutton et al., 2004). The direct correlation of the RNA replication efficiency and infectivity of IBV with the stability of the nsp9 homodimer confirms that dimer is the functional form of the protein. Interestingly, the functionally active unit of the coronavirus $3CL^{pro}$ is also a dimeric form of the protein (Anand et al., 2003).

A recent study by Ponnusamy et al. (2008) reported that HCoV-229E nsp9 forms a different homodimer from SARS-CoV nsp9, in spite of a sequence identity of 45% between the two proteins. In HCoV-229E nsp9, dimerization is mediated by a disulfide bridge, a few hydrogen bonds, and hydrophobic interaction between the C-terminal helix of each monomer. The structural difference between HCoV-229E and SARS-CoV nsp9 may be due to the presence of extra residues from the cloning procedure at the N-terminus of the SARS-CoV nsp9 preparation used for structure determination, which could result in different homodimer forms and different biological functions of proteins. In this study, we observed that the six His-tags in the N-terminus of IBV Nsp9 rendered drastic effects on dimerization and RNA-binding activity of the protein. The six-His tag was removed by factor Xa from all wild type and mutant constructs in our biochemical studies of the protein.

HCoV-229E nsp9 has a Cys (Cys 69) residue in the alpha helix at the homodimer interface and forms a disulfide bridge. This form of nsp9 dimer can bind to single-stranded RNA more tightly and therefore promote replication of the viral genome (Ponnusamy et al. 2008). The SARS-CoV nsp9 has three Cys residues and one of them (Cys 73) is corresponding to Cys 69 in HCoV-229E nsp9. However, these residues are not involved in the formation of intermolecular disulfide bond (Ponnusamy et al. 2008). As the number and position of Cys residues in IBV nsp9 are completely conserved with SARS-CoV nsp9, the IBV nsp9 may form dimer mainly through hydrophobic interaction similar to SARS-CoV nsp9 rather than through formation of a disulfide bridge.

It is intriguing that mutation of the G98 residue to an Asp totally blocks the dimerization and RNA-binding activity of the protein. As explained, no infectious virus was recovered from cells transfected with G98D mutant transcripts. Evidence present suggests that G98D mutation may lead to the disruption of subgenomic RNA transcription and the protein is therefore directly involved in the viral replication. As the RNA-binding assay used in this study involves binding of RNA probes to the denatured, momomeric form of the nsp9 protein, it is quite unlikely that the loss of RNA-binding activity for this mutant is the direct consequence of destabilization of the nsp9 homodimer by this point mutation. One possibility is that the C-terminal domain is directly involved in the binding of RNA. Alternatively, this point mutation may alter the overall folding of the protein.

Nsp9 protein is a nucleic acid-binding protein. The structural characteristics of nsp9 suggested that its nucleic acid-binding activity is not strictly sequence-specific (Egloff et al., 2004; Sutton et al., 2004). The nsp9 protein may bind RNA through wrapping of the ssRNA around the nsp9 dimer (Egloff et al., 2004; Sutton et al., 2004). In this study, we show that mutations of some positively charged residues in the β-barrel regions could significantly reduce the RNA-binding activity of the protein. However, introduction of the same mutations into the viral genome showed only mild or moderate effects on the growth and infectivity of the rescued mutant viruses, though positive correlation between the lowered binding activity and the reduced infectivity of the mutant viruses was observed. It seems that mutations that destabilized the nsp9 homodimer render more profound effect on IBV infectivity than mutations that reduced the RNA-binding activity of the protein per se. We are currently uncertain if this may reflect the limitation of the assay used to analyze the RNA-binding activity of the protein in the study. On the other hand, it would suggest that formation of the nsp9 homodimer may play functions not directly related to the RNA-binding activity of the protein. One possibility is that dimerization of the protein may facilitate its interaction with other viral replicase proteins or host cell proteins involved in the viral replication cycle.

Nsp9 is a putative component of the replication complex. In cells infected with MHV, nsp9 is localized in the perinuclear region together with other proteins of the replication complex (Bost et al., 2000). RdRp was shown to coimmunoprecipitate with $3CL^{pro}$, nsp8 and nsp9 (Brockway et al., 2003). Biophysical evidence has also been presented for an interaction between nsp9 and nsp8 of MHV (Sutton et al., 2004). Interaction between other replicase proteins was also documented. For example, a co-crystal structure of SARS-CoV nsp7 with nsp8 revealed a complex of eight monomers of each protein forming a hollow cylindrical structure. This hexadecameric assembly was proposed to be able to encircle an RNA template, possibly acting as a processivity factor for the RNA polymerase (Zhai et al., 2005). Structural analysis indicated that nsp9 may play multiple roles in coronavirus replication cycle, and its interaction with other proteins may be essential for the formation of the viral replication complex together with its ability to interact with RNA (Egloff et al., 2004; Sutton et al., 2004). However, we were unable to demonstrate direct interaction between IBV nsp9 and the two putative essential components of the replication complex, RdRp and RNA helicase in the overexpression system (data not shown). It suggests that formation of the replication complex may involve other viral and host cell components, including the viral RNA template. Further study would be required to address this interesting issue.

Materials and methods

Cells and cell culture

HeLa and Vero cells were cultured in complete Dulbecco's modified Eagle's medium (Invitrogen) supplemented with 10% newborn calf serum (Sterile) and 1% penicillin (Invitrogen) and maintained at 37 °C in 5% CO_2.

Transient expression of viral protein in mammalian cells

Wild type and mutant IBV nsp9 sequences were placed under the control of a T7 promoter and transiently expressed in mammalian cells using a vaccinia virus-T7 system. Briefly, semiconfluent monolayers of HeLa cells were infected with 10 plaque forming units/cells of recombinant vaccinia virus (vTF7-3), which expresses the T7 RNA polymerase gene, for 2 h at 37 °C prior to transfection. The plasmid DNA was transfected into vTF7-3-infected cells using Effectene transfection reagent according to the manufacturer's instructions (Qiagen). Cells were harvested at 12 to 24 h post-transfection.

Expression, purification and characterization of IBV nsp9 protein in E. coli

His-tagged wild type and mutant nsp9 proteins were expressed in *E. coli* BL-21 by induction with 1 mM isopropyl-b-D-thiogalactopyranoside (IPTG). Cells were lysed by sonication, purified by metal

affinity chromatography with Protino-Ni 150 kit (Macherey Nagel). The purified nsp9-His fusion protein was digested with Factor Xa (Qiagen) overnight at 25 °C with 1.0 U/40 μl of Factor Xa to the purified fusion protein in reaction buffer containing 20 mM Tris–Cl, pH 6.5; 50 mM NaCl; 1 mM $CaCl_2$. After digestion, Factor Xa was removed by affinity chromatography with Xa Removal Resin (Qiagen). Any uncleaved His tag fusion protein remaining after 24 h of digestion was removed by rebinding the sample to Protino-Ni105 column (Macherey Nagel).

Co-immunoprecipitation

Transiently transfected HeLa cells in 60-mm dishes were lysed in 1 ml of lysis buffer (150 mM NaCl, 1% NP-40, and 50 mM Tris–HCl, pH 8.0) with 0.5% protease inhibitor cocktail (Sigma). The lysates were centrifuged at 12,000 rpm for 30 min at 4 °C. The supernatants were added with anti-Flag (Biomed Diagnostics) antibodies at 4 °C for 2 h. Protein-A agarose beads (30 μl) (KPL) were added to the lysates and incubated with shaking for 1 h at 4 °C. The beads were collected by centrifugation and washed for three times with RIPA buffer (150 mM NaCl, 1% NP-40, 0.5% sodium deoxycholate, 0.05% SDS, and 50 mM Tris–HCl, pH 8.0). Proteins binding to the beads were eluted by adding 2×SDS loading buffer and analyzed by Western blotting with anti-Flag or anti-Myc antibody.

Northwestern blot

PCR fragments covering the IBV genome from 27,100 to 27,608 nucleotides were cloned into a plasmid pGEM in either forward or reverse orientation under the control of a T7 promoter. The Dig-labeled sense (+) and anti-sense (−) RNA probes were made in vitro using the DIG RNA labeling kit according to the instructions of the manufacturer (Roche).

Three micrograms of purified proteins was resolved on an SDS-15% polyacrylamide gel and transferred onto nitrocellulose membranes (Hybond C-Extra, Amersham Biosciences) using a semi-dry transfer apparatus. Membranes were washed for 10 min with the probe buffer (1×Denhardt's Reagent, 1 mM EDTA, 10 mM Tris–HCl (pH 7.5) and 50 mM NaCl), blocked for 1 h with 25 mg/ml yeast tRNA (Ambion) and subsequently incubated with 10 mg of DIG-labeled RNA probe in the same probe buffer for 1 h. Membranes were washed three times for 15 min each with the probe buffer, before proceeding to detection with CDP-Star (Roche) according to the manufacturer's instructions.

Chemical cross-linking assay

To investigate the multimeric features of nsp9 protein, the chemical cross-linking experiment was carried out. Wild type and mutate nsp9 protein were purified by gel filtration column and digested by DNAase and RNAase to get rid of the possible binding nucleic acids. Glutaraldehyde (25%, Sigma) was diluted to a series of concentrations (2%, 4%, 8%, 10%, 20%) by distilled water. The protein in PBS buffer was reacted with glutaraldehyde at 16 °C for 30 min. The reaction was stopped by adding SDS PAGE loading buffer and heated at 100 °C for 10 min.

Size-exclusion chromatography assay

The gel-filtration assay was performed for further investigating nsp9 protein multimeric features using BioSuite™ 250 HR SEC column (7.8×300 mm, Waters) on Shimadszu chromatograph (LC-10ATvp) equipped with a photodiode array detector (SPD-M20A). The column was equilibrated at a flow rate of 1 ml/min with PBS buffer at room temperature. The protein sample (300 μl) was injected at a given concentration and detected.

Construction of an infectious IBV clone, introduction of mutations into the clones and rescue of recombinant viruses

Construction of an infectious IBV clone was carried out as described (Tan et al., 2006; Fang et al., 2007). Briefly, five fragments spanning the entire IBV genome were obtained by RT-PCR from Vero cells infected with the Vero cell-adapted IBV p65. The PCR products were purified from agarose gels and cloned into pCR-XL-TOPO (Invitrogen) or pGEM-T Easy (Promega) vectors. Subsequently, fragment A was removed from pCR-XL-TOPO by digestion with NheI and EcoRI, and subcloned into pKT0 vector. Plasmids were digested with either BsmBI (fragment A) or BsaI (fragments B, C, D and E). The digested plasmids were separated on 0.8% agarose gels containing crystal violet. Bands corresponding to each of the fragments were cut from the gels and purified with QIAquick gel extraction kit (QIAGEN Inc.). Fragments A and B, and fragments C, D and E were first ligated with T4 DNA ligase at 4 °C overnight. The two reaction mixtures were then mixed and further ligated at 4 °C overnight. The final ligation products were extracted with phenol/chloroform/isoamyl alcohol (25:24:1), precipitated with ethanol and detected by electrophoresis on 0.4% agarose gels. Full-length transcripts were generated in vitro using the mMessage mMachine T7 kit (Ambion, Austin, TX). The N transcripts were generated by using a linearized pKTO-IBVN containing IBV N gene and the 3′-untranslated region (3′-UTR) as templates. The in vitro synthesized full-length and N transcripts were treated with DNase I and purified with phenol/chloroform. Vero cells were grown to 90% confluence, trypsinized, washed twice with cold phosphate-buffered saline (PBS), and resuspended in PBS. RNA transcripts were added to 400 μl of Vero cell suspension in an electroporation cuvette, and electroporated with one pulse at 450 V, 50 μF with a Bio-Rad Gene Pulser II electroporator. The transfected Vero cells were cultured overnight in 1% FBS-containing MEM in a 60 mm dish or a 6-well plate and further cultured in MEM without FBS. Mutations were introduced into the corresponding fragments by using QuickChange site-directed mutagenesis kit (Stratagene), and confirmed by sequencing of the whole fragments.

Growth curve and plaque sizes of the recombinant viruses on Vero cells

Confluent monolayers of Vero cells on 6-well plates were infected with wild-type and mutant viruses at a multiplicity of ~1 PFU/cell. After 1 h of incubation at 37 °C, cells were washed twice with PBS and cultured in 3 ml of MEM containing 0.5% carboxymethy cellulose for 3 days. The cells were fixed and stained with 0.1% toluidine.

Vero cells were infected with wild-type and recombinant IBV, and harvested at different times post-infection. Viral stocks were prepared by freezing/thawing of the cells three times. The plaque-forming units per ml of each sample were determined by infecting Vero cells on 6-well plates in duplicate with 10-fold serial dilution of each viral stock.

Structure predication of IBV nsp9

JIGSAW server, MOLMOL and PYMOL viewer were used to predict the tertiary structure of IBV nsp9.

Construction of plasmids

PCR products covering the IBV sequence from 11,542 to 11,880 nucleotides were amplified by using the forward primer 5′-CGCGGATCCAATAATGAGCTTATGCCA-3′ and the reverse primer 5′-CCGCTCGAGCTAAGACTGTAAGACAAC-3′. The PCR fragments were digested with BamHI and XhoI, and ligated into BamHI and XhoI digested pXL40 to form plasmid pXL-nsp9. For the plasmid pET-nsp9, the IBV sequence from 11,542 to 11,880 nucleotides was amplified by using the forward primer 5′-GGGAATTCCATATGAATAATGAGCT-TATGCCA-3′ and the reverse primer 5′-CGCGGATCCTTAAGACTGTAA-

GACAACAAC-3′. The PCR fragments were digested with NdeI and BamHI, and ligated into plasmid pET-16 which was digested by NdeI and BamHI, to form plasmid pET-nsp9. Each mutation was introduced by two rounds of PCR and the mutation introduced was confirmed by automated nucleotide sequencing.

References

Anand, K., Palm, G.J., Mesters, J.R., Siddell, S.G., Ziebuhr, J., Hilgenfeld, R., 2002. Structure of coronavirus main proteinase reveals combination of a chymotrypsin fold with an extra alpha-helical domain. EMBO J. 21, 3213–3224.

Anand, K., Ziebuhr, J., Wadhwani, P., Mesters, J.R., Hilgenfeld, R., 2003. Coronavirus main proteinase (3CLpro) structure: basis for design of anti-SARS drugs. Science 300, 1763–1767.

Berman, H.M., Westbrook, J., Feng, Z., Gilliland, G., Bhat, T.N., Weissig, H., Shindyalov, I.N., Bourne, P.E., 2000. The Protein Data Bank. Nucleic Acids Res. 28, 235–242.

Bost, A.G., Carnahan, R.H., Tao Lu, X., Denison, M.R., 2000. Four proteins processed from the replicase gene polyprotein of mouse hepatitis virus colocalize in the cell periphery and adjacent to sites of virion assembly. J. Virol. 74, 3379–3387.

Boursnell, M.E.G., Brown, T.D.K., Foulds, I.J., Green, P.F., Tomley, F.M., Binns, M.M., 1987. Completion of the sequence of the genome of the coronavirus avian infectious bronchitis virus. J. Gen. Virol. 68, 57–77.

Brockway, S.M., Clay, C.T., Lu, X.T., Denison, M.R., 2003. Characterization of the expression, intracellular localization, and replication complex associated with the putative mouse hepatitis virus RNA-dependent RNA polymerase. J. Virol. 77, 10515–10527.

Egloff, M-P., Ferron, F., Campanacci, V., Longhi, S., Rancurel, C., Dutartre, H., Snijder, E.J., Gorbalenya, A.E., Cambillau, C., Canard, B., 2004. The severe acute respiratory syndrome coronavirus replicative protein nsp9 is a single-stranded RNA-binding subunit unique in the RNA virus world. Proc. Natl. Acad. Sci. U. S. A. 101, 3792–3796.

Fang, S.G., Chen, B., Tay, F.P.L., Liu, D.X., 2007. An arginine-to-proline mutation in a domain with undefined function within the RNA helicase protein (NSP13) is lethal to the coronavirus infectious bronchitis virus in cultured cells. Virology 358, 136–147.

Gosert, R., Kanjanahaluethai, A., Egger, D., Bienz, K., Baker, S.C., 2002. RNA replication of mouse hepatitis virus takes place at double-membrane vesicles. J. Virol. 76, 3697–3708.

Imbert, I., Guillemot, J.C., Bourhis, J.M., Bussetta, C., Coutard, B., Egloff, M.P., Ferron, F., Gorbalenya, A.E., Canard, B., 2006. A second, non-canonical RNA-dependent RNA polymerase in SARS coronavirus. EMBO J. 25, 4933–4942.

Joseph, J.S., Saikatendu, K.S., Subramanian, V., Neuman, B.W., Brooun, A., Griffith, M., Moy, K., Yadav, M.K., Velasquez, J., Buchmeier, M.J., Stevens, R.C., Kuhn, P., 2006. Crystal structure of nonstructural protein 10 from the SARS coronavirus reveals a novel fold with two zinc-binding motifs. J. Virol. 80, 7894–7901.

Lim, K.P., Liu, D.X., 1998a. Characterization of a papain-like proteinase domain encoded by ORF1a of the coronavirus IBV and determination of the C-terminal cleavage site of an 87 kDa protein. Adv. Exp. Med. Biol. 440, 173–184.

Lim, K.P., Liu, D.X., 1998b. Characterization of the two overlapping papainlike proteinase domains encoded in gene 1 of the coronavirus infectious bronchitis virus and determination of the C-terminal cleavage site of an 87 kDa protein. Virology 245, 303–312.

Lim, K.P., Ng, L.F., Liu, D.X., 2000. Identification of a novel cleavage activity of the first papain-like proteinase domain encoded by open reading frame 1a of the coronavirus avian infectious bronchitis virus and characterization of the cleavage products. J. Virol. 74, 1674–1685.

Liu, D.X., Tibbles, K.W., Cavanagh, D., Brown, T.D.K., Brierley, I., 1995. Identification, expression and processing of an 87K polypeptide encoded by ORF1a of the coronavirus infectious bronchitis virus. Virology 208, 47–54.

Liu, D.X., Xu, H.Y., Brown, T.D.K., 1997. Proteolytic processing of the coronavirus infectious bronchitis virus 1a polyprotein: identification of a 10 kDa polypeptide and determination of its cleavage sites. J. Virol. 71, 1814–1820.

Liu, D.X., Shen, S., Xu, H.Y., Wang, S.F., 1998. Proteolytic mapping of the coronavirus infectious bronchitis virus 1b polyprotein: evidence for the presence of four cleavage sites of the 3C-like proteinase and identification of two novel cleavage products. Virology 246, 288–297.

Masters, P.S., 2006. The molecular biology of coronaviruses. Adv. Virus Res. 66, 193–292.

Ng, L.F., Liu, D.X., 1998. Identification of a 24-kDa polypeptide processed from the coronavirus infectious bronchitis virus 1a polyprotein by the 3C-like proteinase and determination of its cleavage sites. Virology 243, 388–395.

Ng, L.F., Liu, D.X., 2000. Further characterization of the coronavirus infectious bronchitis virus 3C-like proteinase and determination of a new cleavage site. Virology 272, 27–39.

Ng, L.F., Liu, D.X., 2002. Membrane association and dimerization of a cysteine-rich, 16-kiloDalton polypeptide released from the C-terminal region of the coronavirus infectious bronchitis virus 1a polyprotein. J. Virol. 76, 6257–6267.

Peti, W., Johnson, M.A., Herrmann, T., Neuman, B.W., Buchmeier, M.J., Nelson, M., Joseph, J., Page, R., Stevens, R.C., Kuhn, P., Wu(thrich, K., 2005. Structural genomics of the severe acute respiratory syndrome coronavirus: nuclear magnetic resonance structure of the protein nsp7. J. Virol. 79, 12905–12913.

Ponnusamy, R., Moll, R., Weimar, T., Mesters, J.R., Hilgenfeld, R., 2008. Variable oligomerization modes in coronavirus non-structural protein 9. J. Mol. Biol. 2008 Jul 30 [Electronic Publication ahead of print].

Prentice, E., Jerome, W.G., Yoshimori, T., Mizushima, N., Denison, M.R., 2004. Coronavirus replication complex formation utilizes components of cellular autophagy. J. Biol. Chem. 279, 10136–10141.

Ratia, K., Saikatendu, K.S., Santarsiero, B.D., Barretto, N., Baker, S.C., Stevens, R.C., Mesecar, A.D., 2006. Severe acute respiratory syndrome coronavirus papain-like protease: structure of a viral deubiquitinating enzyme. Proc. Natl. Acad. Sci. U. S. A. 103, 5717–5722.

Ricagno, S., Egloff, M.P., Ulferts, R., Coutard, B., Nurizzo, D., Campanacci, V., Cambillau, C., Ziebuhr, J., Canard, B., 2006. Crystal structure and mechanistic determinants of SARS coronavirus nonstructural protein 15 define an endoribonuclease family. Proc. Natl. Acad. Sci. U. S. A. 103, 11892–11897.

Saikatendu, K.S., Joseph, J.S., Subramanian, V., Clayton, T., Griffith, M., Moy, K., Velasquez, J., Neuman, B.W., Buchmeier, M.J., Stevens, R.C., Kuhn, P., 2005. Structural basis of severe acute respiratory syndrome coronavirus ADP-ribose-1″-phosphate dephosphorylation by a conserved domain of nsp3. Structure 13, 1665–1675.

Shi, S.T., Schiller, J.J., Kanjanahaluethai, A., Baker, S.C., Oh, J.W., Lai, M.M.C., 1999. Colocalization and membrane association of murine hepatitis virus gene 1products and de novo-synthesized viral RNA in infected cells. J. Virol. 73, 5957–5969.

Sims, A.C., Ostermann, J., Denison, M.R., 2000. Mouse hepatitis virus replicase proteins associate with two distinct populations of intracellular membranes. J. Virol. 74, 5647–5654.

Su, D., Lou, Z., Sun, F., Zhai, Y., Yang, H., Zhang, R., Joachimiak, A., Zhang, X.C., Bartlam, M., Rao, Z., 2006. Dodecameric structure of severe acute respiratory syndrome coronavirus nonstructural protein nsp10. J. Virol. 80, 7902–7908.

Sutton, G., Fry, E., Carter, L., Sainsbury, S., Walter, T., Nettleship, J., Berrow, N., Owens, R., Gilbert, R., Davidson, A., Siddell, S., Poon, L.L.M., Diprose, J., Alderton, D., Walsh, M., Grimes, J.M., Stuart, D.I., 2004. The nsp9 replicase protein of SARS-coronavirus, structure and functional insights. Structure 12, 341–353.

Tan, Y.W., Fang, S., Fan, H., Lescar, J., Liu, D.X., 2006. Amino acid residues critical for RNA-binding in the N-terminal domain of the nucleocapsid protein are essential determinants for the infectivity of coronavirus in cultured cells. Nucleic Acids Res. 34, 4816–4825.

Xu, H.Y., Lim, K.P., Shen, S., Liu, D.X., 2001. Further identification and characterization of novel intermediate and mature cleavage products released from the ORF 1b region of the avian coronavirus infectious bronchitis virus 1a/1b polyprotein. Virology 288, 212–222.

Yang, H., Yang, M., Ding, Y., Liu, Y., Lou, Z., Zhou, Z., Sun, L., Mo, L., Ye, S., Pang, H., Gao, G.F., Anand, K., Bartlam, M., Hilgenfeld, R., Rao, Z., 2003. The crystal structures of severe acute respiratory syndrome virus main protease and its complex with an inhibitor. Proc. Natl. Acad. Sci. U. S. A. 100, 13190–13195.

Zhai, Y., Sun, F., Li, X., Pang, H., Xu, X., Bartlam, M., Rao, Z., 2005. Insights into SARS-CoV transcription and replication from the structure of the nsp7–nsp8 hexadecamer. Nat. Struct. Mol. Biol. 12, 980–986.

Ziebuhr, J., 2005. The coronavirus replicase. Curr. Top. Microbiol. Immunol. 287, 57–94.

Ziebuhr, J., Snijder, E.J., Gorbalenya, A.E., 2000. Virus-encoded proteinases and proteolytic processing in the Nidovirales. J. Gen. Virol. 81, 853–879.